Periodic Density Functional Theory Study of the Dissociative Adsorption of Molecular Oxygen over La_2O_3

Michael S. Palmer and Matthew Neurock*

Department of Chemical Engineering, University of Virginia, Charlottesville, Virginia 22904

Michael M. Olken

Corporate Research − Chemical Sciences, The Dow Chemical Company, Midland, Michigan 48674

Received: February 21, 2002

Results of spin-polarized, gradient-corrected, periodic density functional theory calculations are reported for the dissociative adsorption of molecular oxygen over the oxide surface of La_2O_3(001). The diatomic surface oxygen species formed from O_2 dissociation are characterized structurally by a bent orientation with respect to the surface and an $O_{surface}$—O bond length of 1.47 Å; both attributes are consistent with structural features characteristic of classical peroxides. The overall reaction energy for O_2 dissociation into surface peroxide species was calculated to be endothermic by only 12.1 kcal/mol. Several reaction pathways leading to the product were examined; the lowest energy path identified involves a three-center transition state and has an apparent activation barrier of 33.0 kcal/mol. We comment on the role that peroxide species may play in the C—H bond activation step of catalytic oxidative coupling of methane.

Introduction

Research has shown that oxidative coupling of methane (OCM) is a viable method to convert natural gas into valuable liquid products. It is widely accepted that catalytic OCM occurs via a combination of heterogeneous and homogeneous steps. Initial activation of a C—H bond of methane takes places over a metal-oxide surface to produce $\cdot CH_3$ radicals. The methyl radicals recombine in the gas phase to form higher hydrocarbons.[1−5]

Rare-earth-metal (REM) oxides are among the most active catalysts for OCM,[6,7] and a number of experimental studies centered around the mechanistic features of their chemistry have been reported. Although there remains debate as to the nature of the surface species responsible for initial C—H bond activation, Lunsford and co-workers have clearly shown that molecular oxygen is required in order to maintain high levels of catalytic OCM activity.[8] The exact role of O_2 in the chemistry is unclear, but isotopic labeling experiments[9−12] and kinetic studies[13] both suggest that O_2 dissociatively adsorbs over the oxide surface, possibly generating the active oxygen species. To describe the activation of O_2 over oxide surfaces, as well as the nature of the surface oxygen species generated by dissociation, we report here results of periodic density functional theory calculations for the dissociative adsorption of molecular oxygen over La_2O_3(001). The results suggest that dissociative adsorption of O_2 leads to the formation of surface peroxide (O_2^{2-}) sites. It is speculated that peroxide intermediates are responsible for alkane activation on REM oxide catalysts during OCM.

Calculational Details

General Theory. All calculations reported herein were performed using spin-polarized, gradient-corrected, periodic density functional theory (DFT) as implemented in the Vienna ab initio simulation package (VASP).[14−18] Exchange and correlation corrections were described within the generalized gradient approximation of Perdew and Wang (PW91).[19] The La atom was described by the PAW pseudopotential of Kresse.[20] The oxygen atom was described by the Vanderbilt ultrasoft pseudopotential generated by Kresse and Hafner.[21] The basis set was restricted to plane waves with a maximum kinetic energy E_{cut} = 396 eV. Brillouin zone sampling was based on the Monkhörst−Pack scheme,[22] and convergence of the total energy with respect to *k*-point sampling was accelerated for the insulating La_2O_3 by the tetrahedron method with quadratic corrections. A 3 × 5 × 1 Monkhörst−Pack *k*-point grid was used to model the first Brillouin zone. Extensive testing showed that these parameters result in convergence to within 2 meV.

Surface Construction. La_2O_3 crystallizes in the hexagonal space group $P\bar{3}m1$ ($a = b = 3.939$, $c = 6.136$), with a structure characteristic of other A-type sesquioxides. The calculated equilibrium PW91 lattice constants for bulk La_2O_3 are $a = b =$ 3.95 Å and $c = 6.15$ Å, which are in good agreement with the experimental values. The La_2O_3 surface was modeled with a symmetric, stoichiometric 2 × 1 supercell which was 10 atomic layers thick (four lanthanum layers and six oxygen layers). The slab was constructed by cleaving La_2O_3(001) between adjacent $(LaO')_n^{n+}$ layers to expose O′ and six-coordinate La atoms on both faces (Figure 1). The slabs were separated by a vacuum layer of 12 Å. Because the stoichiometry of the unit cell is maintained, all of the oxygen ions, including those on the surface, can be viewed formally as O^{2-} anions.

O_2 Bond Energy. The calculated bond energy and bond length for gas-phase O_2 are 5.93 eV and 1.24 Å, respectively. The corresponding experimental values are 5.25 eV and 1.21 Å.[23] The differences stem mainly from the error in the energy of the free atoms. However, since the density gradients are much lower for the adsorption systems, the description of the energy differences between the reactant state, transition states, and

* Corresponding author.

10.1021/jp020492x CCC: $22.00
Published on Web 06/04/2002

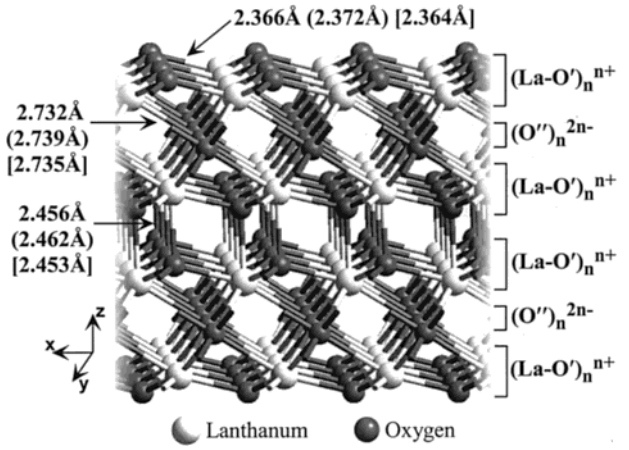

Figure 1. Symmetric, stoichiometric $La_2O_3(001)$ slab. Both faces of the slab expose $(La-O')_n^{n+}$ double hexagonal layers. Bond lengths are for the experimental crystal structure, the bulk structure at the optimized lattice vectors (shown in parentheses), and the relaxed surface structure at the optimized lattice vectors (shown in brackets).

product state is much more accurate than the absolute energy values.

Reaction Energy Calculation. The overall reaction energy was calculated such that the sum of energies of reactants was subtracted from the sum of energies of products (eq 1).

$$\Delta E_{\text{rxn}} = \sum E_{\text{products}} - \sum E_{\text{reactants}} \qquad (1)$$

This convention leads to a negative value for an exothermic reaction. Full relaxation of both the reactant and product state was performed.

O_2 Dissociation. The activation energy for the dissociative adsorption of O_2 was estimated by performing a series of single-point calculations at discrete points on several different 2-dimensional reaction coordinates. Once an approximate activation barrier for dissociation was identified, the O_2 moiety was fixed in space and the surface layers of the La_2O_3 substrate were allowed to relax. The resultant energy was taken to be the approximate activation barrier. Although the VASP code supports "transition state searches" using the Nudged-Elastic-Band (NEB) technique,[24,25] a fully relaxed transition state search was not performed due to the complexity of the system and limited computational resources. The method we employed is considerably less expensive but is not that dissimilar to the NEB technique. The main difference is that the NEB algorithm allows for *full* relaxation of the nuclear positions along the normal to the reaction path. Both methods, however, remain dependent on the choice of reaction pathway. The calculated activation energy from either method should be considered to be an upper bound to the actual barrier. In our case, the limited relaxation could result in a barrier that is overestimated by as much as 5 kcal/mol.

Results and Discussion

Several different reaction pathways leading to the dissociative adsorption of molecular O_2 over $La_2O_3(001)$ were explored. The general features of each O_2 activation site and the respective dissociation route leading to the product state (discussed below) are illustrated in Figure 2. The pathways labeled **1**−**3** involve an O_2 approach that is parallel to the plane of the surface and result in the formation of a four-center transition state in which the O—O bond of the O_2 moiety breaks before either of the surface O′—O bonds form. Sites **1**−**3** differ from one another by their relative position to the underlying La atoms. The

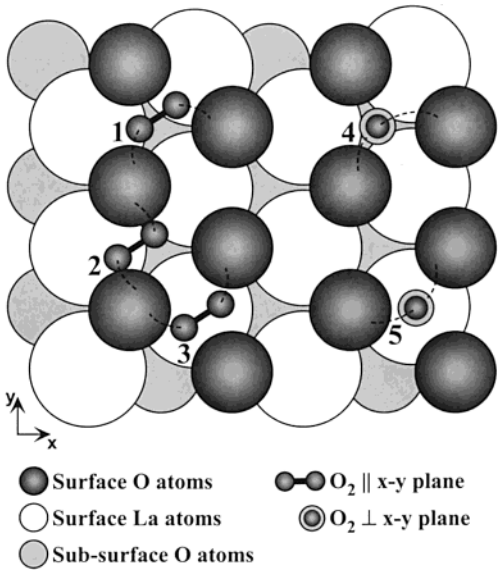

Figure 2. Activation sites and general reaction pathways (illustrated by dashed curves) for the dissociative adsorption of molecular O_2 over $La_2O_3(001)$ that were studied.

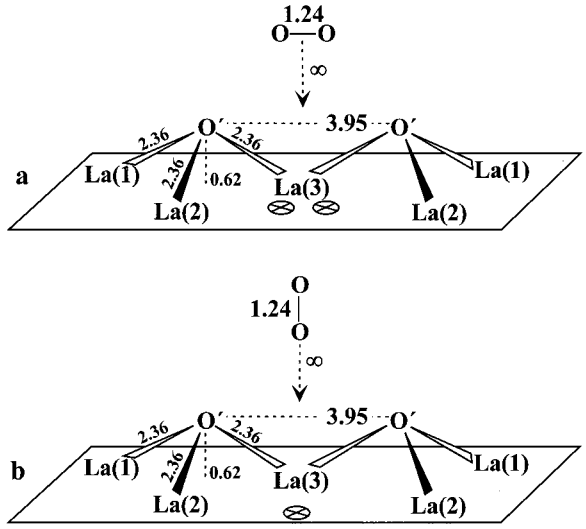

Figure 3. Structural features of the optimized reactant states for the dissociative adsorption of molecular O_2 over $La_2O_3(001)$ described by paths **1** (a) and **4** (b). Only the uppermost surface oxygen (O′) and lanthanum layers (La(1−3)) are depicted. The ⊗ represent the projection of the oxygen atoms of the gas-phase O_2 moiety onto the surface. Distances are in Angstroms.

pathways labeled **4** and **5** involve an O_2 approach that is perpendicular to the plane of the surface and result in the formation of a three-center transition state in which one of the surface O′—O bonds forms before the O—O bond of the O_2 moiety completely breaks. Again, sites **4** and **5** differ from each other by their relative position to the underlying La atoms. The results of our calculations indicate that the systems described by **1** and **4** lead to the lowest activation barriers. The reactant state, product state, and transition state for each of these systems is discussed below in detail. It is worth noting that no pathway involving O_2 dissociation *across the La atoms* near the surface was found to be stable.

Reactant State. The reactant states of **1** and **4** are shown in Figure 3a and 3b, respectively. Both reactant states comprise a clean $La_2O_3(001)$ surface and a gas-phase O_2 molecule at infinite separation from the surface. Geometry optimization of the clean $La_2O_3(001)$ slab did not lead to significant structural changes

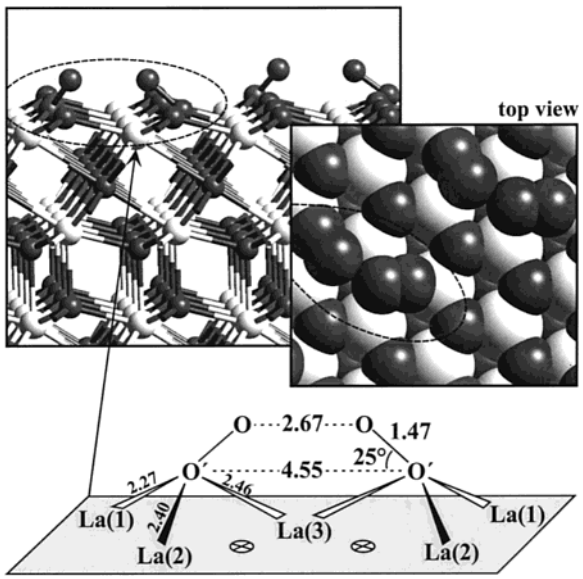

Figure 4. Calculated structure of surface peroxide sites formed by dissociative adsorption of molecular O_2 over $La_2O_3(001)$. The ⊗ represent the projection of the oxygen atoms of the original O_2 moiety onto the surface. Distances are in Angstroms.

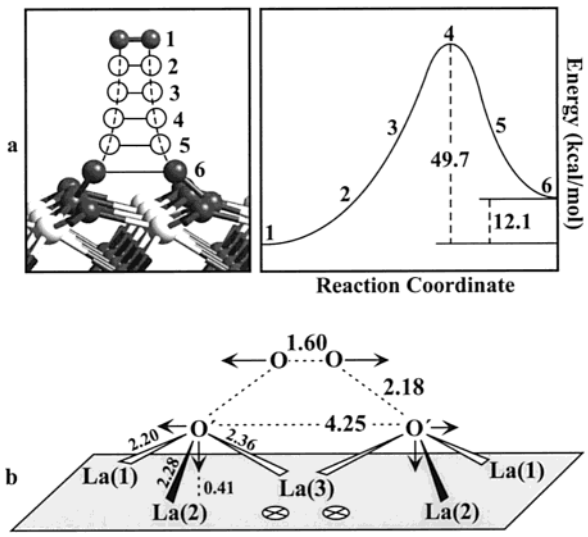

Figure 5. The reaction coordinate (a) and calculated structure of the four-center transition state (b) along route **1** for the dissociative adsorption of molecular O_2 over $La_2O_3(001)$. The arrows in b indicate the motion of the atoms on going from the reactant to the transition state. The ⊗ represent the projection of the oxygen atoms of the original O_2 moiety onto the surface. Distances are in Angstroms.

as compared to the optimized bulk structure; i.e., the short La—O′ bonds are 2.36 Å, the long La—O′ bond is 2.45 Å, the La—O″ bonds are 2.74 Å, and the separation between adjacent surface $(O')^{2-}$ anions is 3.95 Å (refer to Figure 1 for comparison). As expected, the distance from the surface O′ layer and the uppermost La layer contracts slightly from the optimized bulk structure value of 0.65 Å to 0.62 Å. The O—O bond length of the optimized gas-phase O_2 molecule is 1.24 Å.

Product State. The fully optimized product state, formed from the dissociative adsorption of O_2 over $La_2O_3(001)$, is shown in Figure 4. Slight reconstruction of the surface occurs, as evidenced in the contraction of the La(1)—O′ distance and expansion of the La(2)—O′ and La(3)—O′ bond lengths. The surface O′ separation expands from 3.95 to 4.55 Å. The O_2 molecule is completely dissociated, as reflected in an O—O separation of 2.67 Å. The newly formed surface O′—O bonds are 1.47 Å and lie at an angle of approximately 25° with respect to the plane of the surface. The O′ atom is shifted slightly from the 3-fold La site, typical of surface oxide ions and closer to a La-atop site (toward La(1) in Figure 4). This is reflected in a short La(1)—O′ bond length. The reorientation allows the upper oxygen atom of the O′—O surface species to align itself directly above a La—La bridge site (between La(2) and La(3) in Figure 4). The "bent" orientation of the surface species is advantageous over one in which the O_2 moiety lies perpendicular to the surface, since it allows the three underlying La^{3+} cations to help stabilize the negative charge on *both* oxygen atoms of the O_2 moiety rather than only one. The overall energy for the dissociative adsorption of molecular oxygen over the $La_2O_3(001)$ surface is calculated to be only 12.1 kcal/mol.

Transition State. The overall O_2 dissociative adsorption reaction coordinate for the pathway described by **1** is illustrated in Figure 5a. As O_2 is brought close to the surface, the uppermost oxygen layer contracts inward toward the bulk, resulting in a decrease in the La(1)/(2)—O′ bond lengths and a concomitant decrease in the distance between the surface O′ layer and the uppermost La layer. Movement of layers below the surface oxygen layer is negligible. In addition to the contraction of the surface O′ layer, the surface O′ atoms directly below the approaching O_2 moiety separate. Surface reconstruction continues in this manner until the transition state is reached. At the four-center transition state (Figure 5b), the La—O′ bond lengths range from 2.2 to 2.36 Å, the O′ separation is 4.25 Å, and the distance between the surface O′ layer and the uppermost La layer is 0.41 Å. The O—O bond length of the O_2 moiety stretches to 1.60 Å, and the distance between the oxygen atoms of the O_2 moiety and the surface O′ ions is 2.18 Å. The activation barrier for the dissociation process described by **1** is calculated to be 49.7 kcal/mol. The high activation barrier is directly related to the fact that much of the O—O bond of the O_2 moiety is broken while neither of the surface O′—O have formed yet. It is worth noting that no physisorbed state of molecular O_2 was identified along this particular reaction path. This is not surprising, however, given that the O_2 molecule interacts predominantly with the surface oxide ions and the fact the La_2O_3 is an insulating material with a calculated band gap of 3.81 eV.

The overall O_2 dissociative adsorption reaction coordinate for the pathway described by **4** is illustrated in Figure 6a. Similar surface reconstructions to those mentioned above, although not as pronounced, take place as the O_2 molecule is brought near the surface. In contrast to the reaction pathway described by **1**, there exists an O_2 physisorbed state at an O_2—surface separation of approximately 0.1 Å (step 1). This state is stabilized due to the fact that the O_2 moiety is positioned above a 3-fold La^{3+} site (O—La(1)/La(2)/La(3) = 2.82 Å). From the physisorbed state, the upper oxygen atom of the O_2 moiety tilts over and interacts with a surface O′ atom. Expansion of the O_2 bond and repulsive interactions with the surface result in an activated complex with an intrinsic barrier estimated to be less than 25 kcal/mol (step 3). The activated complex leads to a *local* minimum structure along the potential energy surface (step 4). The structure of this intermediate, illustrated in Figure 6b, is located at the point where the O_2 bond is still intact and the first surface O′—O bond is formed. The activated complex leading to complete dissociation of O_2 is illustrated in Figure 6c. At the three-center transition state, the O′ separation is 4.13 Å, and the distance between the surface O′ layer and the uppermost La layer is 0.34 Å. The O—O bond length of the O_2 moiety stretches to 2.00 Å. The distance between the oxygen

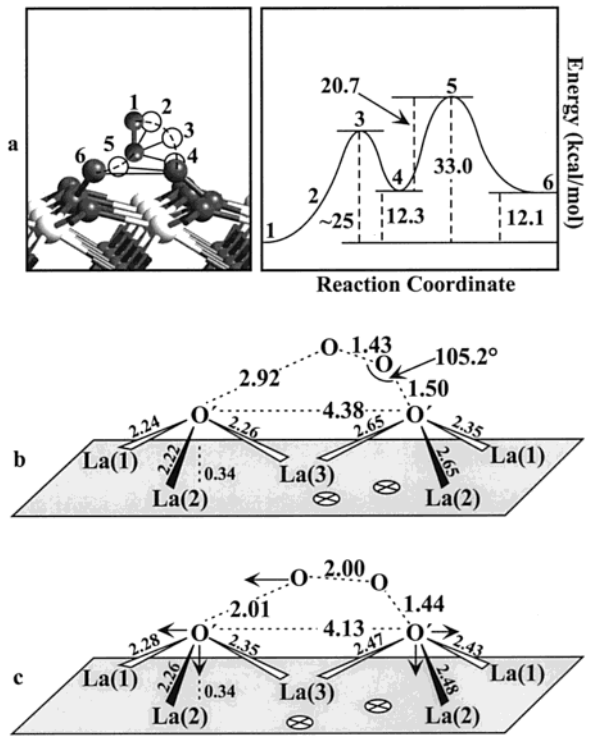

Figure 6. The reaction coordinate (a), calculated structure of the intermediate (b), and calculated structure of the three-center transition state (c) along route **4** for the dissociative adsorption of molecular O_2 over La_2O_3(001). The arrows in c indicate the motion of the atoms on going from the intermediate to the transition state. The ⊗ represent the projection of the oxygen atoms of the original O_2 moiety onto the surface. Distances are in Angstroms.

atoms of the O_2 moiety and the surface O′ ions is 1.44 and 2.01 Å. The intrinsic barrier is calculated to be only 20.7 kcal/mol, while the apparent activation barrier for the entire dissociation process described by path **4** is calculated to be 33.0 kcal/mol. The apparent activation energy is markedly lower than the barrier for **1**, and results from the fact that one of the surface O—O′ bonds is formed before the O_2 molecule completely dissociates and because the "dangling" oxygen atom is stabilized in the 3-fold La^{3+} site.

Strictly as a frame of reference, Mirodatos and co-workers have studied oxygen activation over unsupported lanthana under typical OCM conditions using variable-temperature, oxygen steady-state isotopic transient kinetics experiments.[10] They determined the apparent activation for the O_2 isotopic exchange process to be approximately 24 kcal/mol. They also concluded that "gaseous oxygen activation [reflected in isotope exchange] proceeds dissociatively and involves lattice oxygen." While the activation barrier for oxygen isotope exchange is not necessarily related to that for dissociative adsorption, these experimental results and conclusions are in line with our findings.

General Comments on OCM Chemistry. The calculated bond length of the O′—O surface species of the product state is characteristic of a classical peroxide (1.49 ± 0.02 Å). Despite mounting evidence which supports the role of peroxides as the active OCM species,[26−33] the only other description of a peroxide-like species on OCM catalysts is that of a "nonclassical" peroxide. Nonclassical peroxides have been characterized as a through-bond species involving two isolated yet coupled O^- surface anions. Simulations by Islam and Illet[34,35] on La_2O_3-(011) predicted an O^-—O^- distance of 3.9 Å, and experiments by Lunsford and Kharas on $BaPbO_3$ indicated a O^-—O^- contact of ∼3.0 Å. Lunsford and Kharas[36] noted, however, that crystallographic analysis of $BaPbO_3$ was based on a profile refinement of powder data which included high R-factors. Regardless of the validity of these claims, it is clear from our results that it is not necessary to describe surface peroxide species on La_2O_3 in a nonclassical manner. Based on the calculated apparent activation barrier (33.0 kcal/mol) and overall reaction energy (12.1 kcal/mol) for the dissociative adsorption of O_2, it is reasonable to suggest that classical O_2^{2-} surface species can be formed directly over the La_2O_3 surface under typical OCM operating conditions (600−700 °C). Calculations indicate that these peroxide intermediates are active for the dissociation of a C—H bond of methane. Results of these studies will be described in a another paper.[37]

Acknowledgment. We kindly acknowledge financial support from the Dow Chemical Company. We thank the office for Information Technology and Communication (ITC) at UVa, the Computer Science Department at UVa, and NCSA at the University of Illinois at Urbana-Champaign (Grant CTS 000028N) for valuable computer time. We also thank Dr. Georg Kresse (Institut für MaterialPhysik, Technische Universität Wien) for the La PAW pseudopotential used in our VASP calculations.

References and Notes

(1) Amenomiya, Y.; Birss, V. I.; Goledzinowski, M.; Galuszka, J.; Sanger, A. R. *Catal. Rev. −Sci. Eng.* **1990**, *32*, 163−227.
(2) Dubois, J.-L.; Cameron, C. J. *Appl. Catal.* **1990**, *67*, 49−71.
(3) Lee, J. S.; Oyama, S. T. *Catal. Rev. −Sci. Eng.* **1988**, *30*, 249−280.
(4) Lunsford, J. H. *Angew. Chem., Int. Ed. Engl.* **1995**, *34*, 970−980.
(5) Voskresenskaya, E.; Roguleva, V.; Anshits, A. G. *Catal. Rev. −Sci. Rev.* **1995**, *37*, 101−143.
(6) Campbell, K. D.; Zhang, H.; Lunsford, J. H. *J. Phys. Chem.* **1988**, *92*, 750−753.
(7) Otsuka, K.; Jinno, K.; Morikawa, A. *J. Catal.* **1986**, *100*, 353−359.
(8) Lin, C.-H.; Campbell, K. D.; Wang, J.-X.; Lunsford, J. H. *J. Phys. Chem.* **1986**, *90*, 534−537.
(9) Haung, S.-J.; Walters, A. B.; Vannice, M. A. *J. Catal.* **2000**, *192*, 29−47.
(10) Lacombe, S.; Zanthoff, H.; Mirodatos, C. *J. Catal.* **1995**, *155*, 106−116.
(11) Winter, E. R. S. *J. Chem. Soc. A* **1969**, 1832−1835.
(12) Winter, E. R. S. *J. Chem. Soc. A* **1969**, 2889−2902.
(13) Pak, S.; Qiu, P.; Lunsford, J. H. *J. Catal.* **1998**, *79*, 222−230.
(14) Kresse, G.; Hafner, J. *Phys. Rev. B* **1993**, *47*, 558−561.
(15) Kresse, G.; Hafner, J. *Phys. Rev. B* **1994**, *49*, 14251−14269.
(16) Kresse, G.; Furthmüller, J. *Phys. Rev. B* **1996**, *54*, 11169−11186.
(17) Kresse, G.; Furthmüller, J. *Comput. Mater. Sci.* **1996**, *6*, 15.
(18) Moroni, E. G.; Kresse, G.; Hafner, J.; Furthmüller, J. *Phys. Rev. B* **1997**, *56*, 15629−15646.
(19) Perdew, J. P.; Chevary, J. A.; Vosto, S. H.; Jackson, K. A.; Pederson, M. R.; Singh, D. J.; Frolhais, C. *Phys. Rev. B* **1992**, *46*, 6671−6687.
(20) Kresse, G., personal correspondence.
(21) Kresse, G.; Hafner, J. *J. Phys.: Condens. Matter* **1994**, *6*, 8245−8257.
(22) Monkhörst, H. J.; Pack, J. D. *Phys. Rev. B* **1976**, *13*, 5188−5192.
(23) *Handbook of Chemistry and Physics*, 82nd ed.; Lide, D. R., Ed.; CRC Press: Boca Raton, FL 2001.
(24) Mills, G.; Jonsson, H. *Phys. Rev. Lett.* **1994**, *72*, 1124.
(25) Mills, G.; Jonsson, H.; Schenter, G. K. *Surf. Sci.* **1995**, *324*, 305.
(26) Otsuka, K.; Said, A. A.; Jinno, K.; Komatsu, T. *Chem. Lett.* **1987**, 77−80.
(27) Otsuka, K.; Murakami, Y.; Wada, Y.; Said, A. A.; Morikawa, A. *J. Catal.* **1990**, *121*, 122−130.
(28) Sinev, M. Y.; Korchak, V. N.; Krylov, O. V. *Kinet. Katal.* **1986**, *27*, 1274.
(29) Lunsford, J. H.; Yang, X.; Haller, K.; Laane, J. *J. Phys. Chem.* **1993**, *97*, 13810−13813.
(30) Dissanayake, D.; Lunsford, J. H.; Rosynek, M. P. *J. Catal.* **1993**, *143*, 286−298.
(31) Yamashita, H.; Machida, Y.; Tomita, A. *Appl. Catal.: A General* **1991**, *79*, 203−214.
(32) Mestl, G.; Knozinger, H.; Lunsford, J. H. *Ber. Bunsen-Ges. Phys. Chem.* **1993**, *97*, 319−321.

(33) Au, C. T.; He, H.; Lai, S. Y.; Ng, C. F. *J. Catal.* **1996**, *163*, 399−408.
(34) Islam, M. S.; Ilett, D. J.; Parker, S. C. *J. Phys. Chem.* **1994**, *98*, 9637−9641.
(35) Islam, M. S.; Ilett, D. J. *Catal. Today* **1994**, *21*, 417−422.
(36) Kharas, K. C. C.; Lunsford, J. H. *J. Am. Chem. Soc.* **1989**, *111*, 2336−2337.
(37) Palmer, M. S.; Neurock, M.; Olken, M., *J. Am. Chem. Soc.*, in press.